

Electronic, Elastic and X-ray spectroscopic properties of direct and inverse full Heusler compounds: DFT+U study

Lalrinkima,¹ Gennady M. Mikhailov,² and D. P. Rai^{1,*}

¹*Department of Physics, Pachhunga University Collge, Aizawl-796001, India*

²*Institute of Microelectronics Technology and High Purity Materials RAS, 142432 Chernogolovka, Russia*

Half-metallicity, low magnetic damping and high curie temperature (T_C) are crucial for application in spintronics and full Heusler alloys in this regard exhibit remarkable properties. Herein, we have considered Co_2FeAl (CFA) and Fe_2CoAl (FCA) as a representative of direct and indirect full Heusler compounds which crystallizes in $L2_1$ and $C1_b$ phases, respectively. The theory of $L2_1$ type Heusler alloys has been well established, however the fundamental understanding of Fe_2CoAl is still under developed. In this paper, we have employed density functional theory (DFT) to study the electronic, elastic and X-ray spectroscopic properties of Co_2FeAl and Fe_2CoAl . The electron exchange correlation were treated within a generalized gradient approximation (GGA) as PBE-scheme. Inorder to include the impact of valence electrons an onsite Coulomb potential is added to GGA as GGA+U. Within both GGA and GGA+U, CFA shows a half-metallic behaviour but FCA is metallic. The calculated values of magnetic moment and T_C are in close agreement with the experimental data

PACS numbers: Valid PACS appear here???

I. INTRODUCTION

The recent challenges for the material scientists and material engineers is to develop a new and eco-friendly material for the advancement of smart devices. Material science is an open field to accept the new approaches for the technological development. The conventional semiconductor electronic devices works on the basis of electron charge transfer that accomplished by high level of energy consumption. Alternatively, the usage of electron spin-based innovation called spintronics¹⁻⁶ which utilizes the spin degrees of freedom, can give extra functionality and new capabilities, including faster switching time and lower power consumption. The spintronic devices solely rely on the spin polarization at the Fermi energy (E_F) of the material⁷⁻¹⁴. Researchers believed that the future spin based electronic devices outclass the customary charge-based electronic devices in terms of low power consumption, ecologically and efficiency. The spin functionality of electron was successfully implemented in a device as giant-magneto-resistance (GMR) in 1988². One of the potential competitors is transition based Heusler compounds due to the presence of d -orbitals which play an important role in determining the multi-functional properties and their application in diverse field⁷. The transition metal based Heusler alloys show high magnetic moment in the absence of applied magnetic field¹⁵⁻²⁰. The other fascinating feature is their high Curie temperature T_C which is an important criteria for technological application and can be well fabricated in devices preserving the ferromagnetism above the room temperature (RT). The theoretical T_C of some of the well known Co-based Heusler compounds calculated from atomistic spherical wave approximation (ASW)²¹ are Co_2VGa ($T_C=368$ K), Co_2CrGa ($T_C=362$ K), Co_2MnAl ($T_C=609$ K), Co_2MnSi ($T_C=990$ K), Co_2MnSn ($T_C=899$ K) and Co_2FeSi ($T_C=1183$ K). While the experimental²²⁻²⁵ values of T_C for the aforementioned compounds are 352 K, 495 K²⁶, 697 K, 985 K, 1100 K, respectively. Majority of Heusler compounds show high

spin polarization at Fermi level (E_F), due to the presence of conducting electrons that gives dispersed bands around the E_F at one of the spin channels whereas other spin channel is semiconducting with a band gap. The Half-metallic characteristics in Heusler compound is attributed to the hybridization between the $d-d$ orbitals of the transition elements²⁷. The half-metallic Heusler compounds are superior interms of their technological application as compared to other class of half metals like oxides (CrO_2 , Fe_3O_4)²⁸, manganites $\text{La}_{0.7}\text{Sr}_{0.3}\text{MnO}_3$ ²⁸, perovskite $\text{Sr}_2\text{FeReO}_6$ ^{29,30}, pyrites CoS_2 ³¹, chalcogenides CrSe ³², pnictides CrAs ³² etc., due to higher value of T_C and high magnetic moment. The above discussed diverse properties of Heusler compound are highly plausible for the advancement of new spin-based technology^{33,34}. However, the understanding of complex magnetization due to the presence of d -electrons and the distribution of magnetic moments in atomistic-scale is crucial. An insight of the intrinsic magnetic properties can be achieved by using magneto-optical spectroscopy, e.g, the X-ray absorption spectroscopy (XAS) and X-ray magnetic circular dichroism (XMCD)³⁵⁻³⁸. The magneto-optical analysis provide a quantitative information about the local spin and orbital magnetic moments of the 3d atoms in the form of $2p_{1/2,3/2} \rightarrow 3d$ transitions as $L_{2,3}$ absorption edges. The transition metal based Heusler compound constituted strongly correlated electrons which are not accounted within a conventional density functional theory (DFT). Hence, the information obtained are inaccurate and inadequate. In this paper we have implemented DFT+U (Coulomb potential) approach to integrate the impact of the valence electrons (strongly correlated d -electrons) to procure precision in the outcomes.

II. COMPUTATIONAL DETAIL

In general, the full Heusler alloy (FHA) is expressed as X_2YZ , where X and Y are transition elements and Z species is p -elements. There are two types of full-Heusler; direct

and inverse depending on the arrangement of atoms according to their electronegativity. The direct FHA crystallizes in $L2_1$ structure, consisting of four inter-penetrating FCC lattices with space group $225(Fm\bar{3}m)^{39}$. Inverse FHA crystallizes in $C1_b$ type structure having space group $216(F\bar{4}3m)$ where the electronegativities of X and Y are just the reverse as compared to direct one [Fig.1(a,b)]. In this work, we have used an efficient and globally adopted an open source DFT-package called Quantum Espresso⁴⁰. The relaxed structure at its ground state has been achieved by optimizing the lattice parameters based on Murnaghan's equation of states (EOS)⁴¹. For further confirmation of thermodynamical stability we have also calculated the frequency dependent phonon dispersion based on linear response method⁴² in combination with the density functional perturbation theory (DFPT) as program in Quantum Espresso⁴³. Quantum Espresso works on the basis of projected augmented wave (PAW) method that rely on the ultrasoft pseudopotential functional⁴⁴. All electrons are treated by using a generalised gradient approximation (GGA) within Perdew-Burke-Ernzerhof (PBE) functional⁴⁵. A cut-off energy of 50 eV has been considered within a plane wave basis set. The k-points correspond to the electronic wave functions are integrated within a first Brillouin Zone (BZ) by Monkhorst-pack $8 \times 8 \times 8$ ⁴⁶. For the accurate and efficient treatment of the electron-electron interaction among the strongly correlated d-electrons, we have also deployed Hubbard on-site Coulomb interaction (U) within the DFT formalism as GGA+U. The respective U values⁴⁷ of Co and Fe are $U_{Co} = 3.89$ eV and $U_{Fe} = 3.82$ eV, have been adopted for our calculation. We have also computed the X-ray Absorption Spectra (XAS) and X-ray Magnetic Circular Dichroism (XMCD) using the spin-polarized, relativistic Korringa-Kohn-Rostoker method (SPR-KKR)^{48,49}.

III. RESULTS AND DISCUSSION

The optimized lattice constants (a_o) of Co_2FeAl calculated from from GGA and GGA+U are 5.044\AA and 5.7036\AA respectively. Also, the respective values of lattice constants for Fe_2CoAl within GGA and GGA+U are 5.70\AA and 5.73\AA . The calculated lattice parameters in comparison with the previously reported theoretical and experimental data are presented in Table I. Our calculated lattice parameters are in qualitative and in close agreement with the previous results.

Compounds	B*(GPa)	B**(GPa)	a (Å)	a_{Theo}^{Rep} (Å)	a_{Expt} (Å)
CFA-GGA	193.7	209.27	5.704	5.69 ³⁹ , 5.70 ⁵³	5.74 ⁵¹
CFA-GGA+U	110.4		5.746		
FCA-GGA	187.2	208.67	5.703	5.71 ³⁹ , 5.67 ⁵⁴	5.766 ⁵²
FCA-GGA+U	325.0		5.733		

TABLE I. Calculated Lattice Constant a (Å) in comparison with the reported data and the Bulk Modulus (where B* based on Murnaghan's equation⁴¹ and B** from Elastic code⁵⁰)

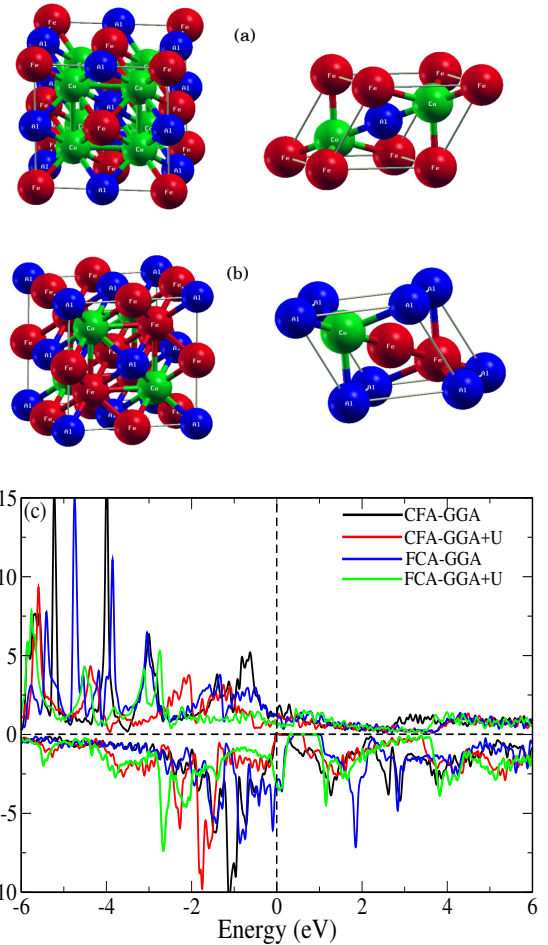


FIG. 1. Conventional and primitive cell of (a) $L2_1$ -type Co_2FeAl , (b) $C1_b$ -type Fe_2CoAl structure and (c) Total density of states (DOS) of Co_2FeAl and Fe_2CoAl calculated from GGA and GGA+U

A. Electronic and Magnetic properties

By using the optimized lattice constant, the electronic and magnetic properties were calculated. The vivid description of the electronic properties of crystalline material is directly related to density of states (DoS) and band structures. Hence, the total DoS of Co_2FeAl and Fe_2CoAl calculated from GGA and GGA+U are shown in Fig.1(c). We have found that the total DoS of Co_2FeAl and Fe_2CoAl are not comparable despite of having similar chemical composition, due to the differences in their crystallization (space group). In case of Fe_2CoAl the Fermi energy (E_F) is completely shifted to the valence region, whereas in Co_2FeAl we can see E_F falling exactly in the band gap in the spin down channel within both GGA and GGA+U approximation. The former exhibits a pure metallic behaviour on the other hand the later gives the half-metallic characteristics. The half metallicity is basically due to the presence of metallic state at one of the spin channels whereas other channel is semiconducting⁵⁵. In Co_2FeAl , Co- $d(\uparrow)$ ($d-e_g+d-$

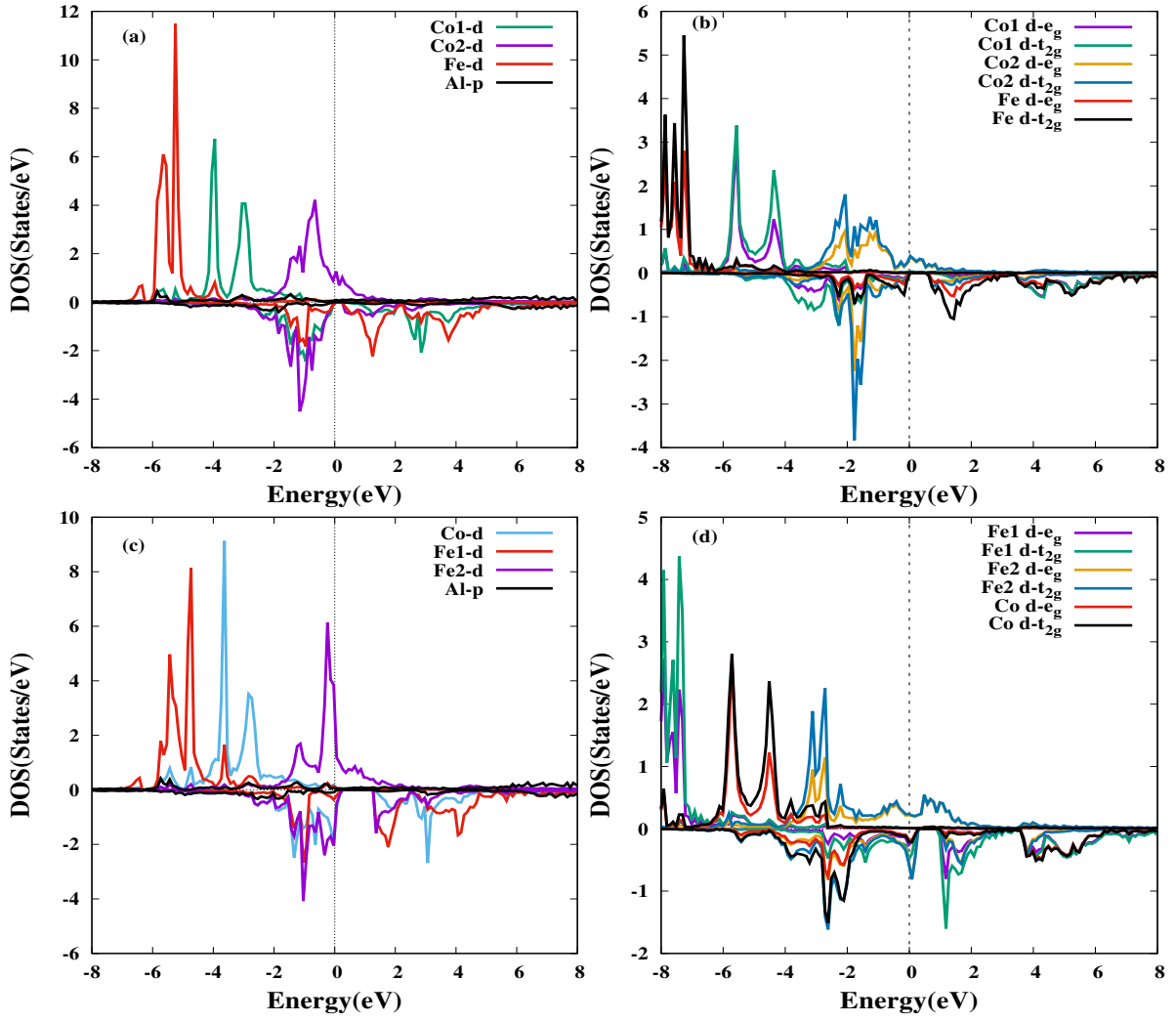


FIG. 2. Calculated partial DoS of Co_2FeAl : (a) GGA, (b) GGA+U and Fe_2CoAl :(c) GGA, (d) GGA+U

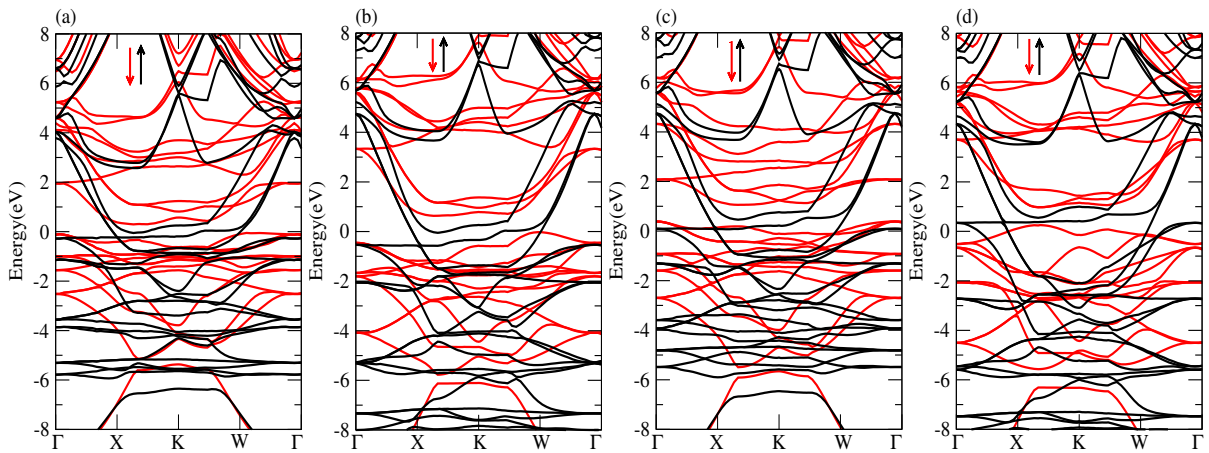


FIG. 3. Calculated band structures of Co_2FeAl : (a) GGA, (b) GGA+U and Fe_2CoAl :(a) GGA, (b) GGA+U

t_{2g}) states are dispersed around the E_F and Fe- $d(\uparrow)$ states are located at around -4.0 eV to -6.0 eV in spin up channel, and a presence of clear band gap at the spin down channel gives all the credibility to its half-metallic behaviour, [Fig.2(a, b)]. The formation of band gap in the spin down channel of Co_2FeAl ascribed to the hybridization between the d -orbitals of transition metal atoms [Fig. 2(a,b)]. The $d-d$ hybridization in $L2_1$ type structure has already been discussed somewhere else²⁷. The $d-d$ hybridization gives bonding (occupied) and anti-bonding (unoccupied) states where bonding states are stable with low energy and shifted below the E_F . The energy difference between the bonding and anti-bonding states is a measure of half-metallic band gap (E_g). The calculated band gap of Co_2FeAl along K-point from GGA and GGA+U are 0.2 eV and 0.51 eV respectively [see Fig. 3(a,b)]. However, the GGA band gap of Co_2FeAl is slightly narrower than that of GGA+U. The degenerated band gap is due to fact that GGA is insufficient in deriving the free electrons efficiently. Rather, the free electrons in the interstitial region are treated as impurities which induced extra states at the edge of the band gap. As a consequence of metal-semiconductor hybrids the E_F lies within the band gap, thus Co_2FeAl exhibit 100% spin polarization. The empirical formula to estimate the degree of spin polarization at E_F ²⁸ is given by Eq. (1)

$$P = \frac{N_{\uparrow}(E_F) - N_{\downarrow}(E_F)}{N_{\uparrow}(E_F) + N_{\downarrow}(E_F)} \quad (1)$$

where $N_{\uparrow}(E_F)$ and $N_{\downarrow}(E_F)$ are the number of density of states at E_F for spin-up and spin-down channels respectively. The partial DoS of Fe_2CoAl is shown in Fig.2(c,d) which predict its metallic characteristic. The band gap in the spin-down channel is located above the Fermi level. As one can see the E_F is passing through the dispersed DoS in both the spin channels, also cross checked from Fig.3(c,d). The total magnetic moment of $L2_1$ and $C1_b$ type Heusler compound is based on the Slater-Pauling (SP) rule⁵⁶. Full-Heusler compound follows the rule of 24; $M_t = Z_t - 24$ (μ_B), where M_t and Z_t are the total magnetic moment and total valence electrons, respectively. The integer value of M_t is another important factor to determine the half-metallic behaviour. The respective values of Z_t for Co_2FeAl and for Fe_2CoAl are 29 and 28. So the expected values of M_t for Co_2FeAl and Fe_2CoAl are 5 (μ_B) and 4 (μ_B), respectively. The calculated $M_t = 5.00 \mu_B$ for Co_2FeAl , exactly an integer value that falls within the SP-rule but $M_t = 5.12 \mu_B$ for Fe_2CoAl deviates abruptly. This is because there are 11.5 electrons instead of 12 in the spin down band and in the majority band there 16.5 electrons instead of 16. This leads to $M_t = 16.5 - 11.5 = 5.00 \mu_B$ instead of $4.00 \mu_B$ in Fe_2CoAl . To restore half metallicity the variation of lattice constant may works well. This will shift the E_F into the band gap and the perfect half-metal with $M_t = 4.00 \mu_B$ may be possible. The calculated M_t values of Co_2FeAl and Fe_2CoAl are presented in Table II along with the previous reports. Our results are in good agreement with the available data. Another interesting feature is high value of Curie temperature (T_C) exhibited by majority of the Heusler compounds. The Curie temperatures (T_C) are calculated from the following Eq. (2)^{57,58}

$$T_C = 23 + 181 \times M_t \quad (2)$$

T_C is strongly related to the total magnetic moment (M_t) thus we can get a linear relation between T_C and M_t (mimic $y = mx + c$) which shows that higher value of M_t gives high T_C . We have also estimated the strength of the magnetic inter-

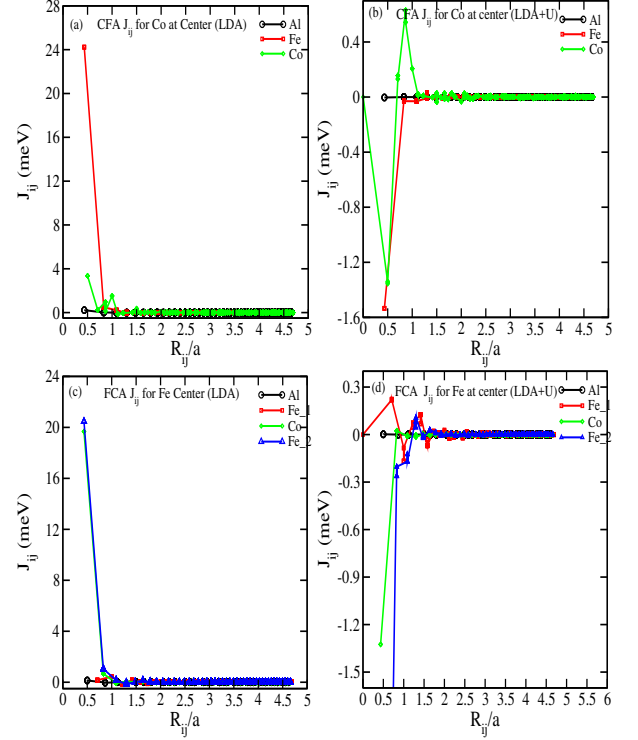


FIG. 4. Calculated exchange coupling J_{ij} parameter of: (a) Co_2FeAl at Co center within LDA (b) Co_2FeAl at Co center within LDA+U, (c) Fe_2CoAl at Fe center within LDA and (d) Fe_2CoAl at Fe center within LDA+U

action by calculating the exchange coupling constants J_{ij} between two atoms at i and j sites as a function of distance [see Fig.4]. According to a classical Heisenberg model the central atoms are embedded in a ferromagnetic coherent potential approximation (CPA) medium and the exchange coupling constants are calculated by mapping the difference of total energy due to minute change in the rotations of the two moments at i and j sites⁵⁹. The exchange coupling J_{ij} is given by

$$J_{ij} = \frac{1}{4\pi} \int^{E_F} d(E) \Im Tr_L \{ \Delta_i T_{\uparrow}^{ij} \Delta_j T_{\downarrow}^{ji} \} \quad (3)$$

where $\Delta_i = t_{i\uparrow}^{-1} - t_{i\downarrow}^{-1}$, $t_{i\uparrow}^{-1}$ is the atomic t -matrix of the of magnetic impurities at site i for the spin up/down state. $T_{\uparrow\downarrow}^{ij}$ is the scattering path operator between ij sites for the spin up/down state. Tr_L is the trace over the orbital variables. The Curie temperature (T_C) can be calculated from the mean field

approximation (MFA) by using Eq.(4).

$$k_B T_C \langle s_i \rangle = \frac{2}{3} c \sum_{j,r \neq 0} J_{ij}^{0,r} \langle s_j \rangle \quad (4)$$

where c is the concentration of impurities and k_B is the Boltzmann constant, $\langle s_j \rangle$ is the average j component of the unit vector s_r^j along the direction of magnetization. The calculated T_C^{MFA} are tabulated in Table II and overestimated because of the inadequate description of the magnetic percolation effect^{60,61}.

IV. X-RAY ABSORPTION SPECTRA (XAS) AND X-RAY MAGNETIC CIRCULAR DICHROISM (XMCD)

A theoretical study of XAS and XMCD have been performed based on the sum rule within the frame work of DFT+U in an absence of external applied field. Fig.5(a,b) shows the calculated XAS and XMCD spectra of Co and Fe at $L_{2,3}$ edges for Co_2FeAl and Fe_2CoAl . The XAS of Co atoms in Co_2FeAl are more sharp with high intensity as compared to Fe atoms. On the other hand the XAS of Fe atoms in Fe_2CoAl shows more intense peaks. The L_3 and L_2 edges are denoted as peak 1 and peak 2 in Fig.5(a,b). The ratio of intensities of XAS, between L_3 and L_2 edges in Co is 2:1 and Fe is 2.4:1 for Co_2FeAl , in good agreement with the experiment⁶². Moreover, the ratio of L_3 and L_2 in Fe_2CoAl is 3:1 for Co and 2.6:1 for Fe atom. The similar result of deviation of branching ratio from standard 2:1 as in later case has also been reported in all one-electron approach^{63,64}. This discrepancy may be because of the implementation of inaccurate Coulomb potential (U_{Co}/U_{Fe}) for electron core-hole exchange correlation in Fe_2CoAl . The $L_{3,2}$ -XAS of Co and Fe are related to the unoccupied d-states near E_F . The L_3 edges in Fig.5(a, b) are derived from the spin-resolved unoccupied Co-d $t_{2g}(\uparrow)$ and Fe-d $t_{2g}(\uparrow)$ states for Co_2FeAl and Fe_2CoAl , respectively [see Fig.2 (b,d)]. These results are in good agreement with the experimental one calculated from the ultra-high vacuum magnetron sputtering by applying pressure below 8×10^{-10} Pa⁶⁵. The absorption peaks at 2 eV and 18 eV are due to the transition of $2p_{3/2} \rightarrow 3d$ and $2p_{1/2} \rightarrow 3d$ which corresponds to L_3 and L_2 edges, respectively. The XMCD spectra are calculated corresponds to XAS. The first XMCD spectra of Co and Fe atoms occur at 0.5 eV but in the second XMCD spectra Co edgeout Fe by ~ 3.0 eV [Fig.5(a)]. The occurrence of XMCD Co- $L_{2,3}$ and Fe- $L_{2,3}$ peaks are in a direct relation to ferromagnetic ordering of Co_2FeAl , which has also been reported earlier^{62,65}. The similar explanation may follows for Fe_2CoAl as well [Fig.5(b)].

V. PHONON PROPERTIES

We have also presented the GGA calculation of lattice dynamics for Co_2FeAl and Fe_2CoAl with the relaxed structure. The graphical representation of the phonon dispersion curve within first Brillouin zone and the phonon density of states

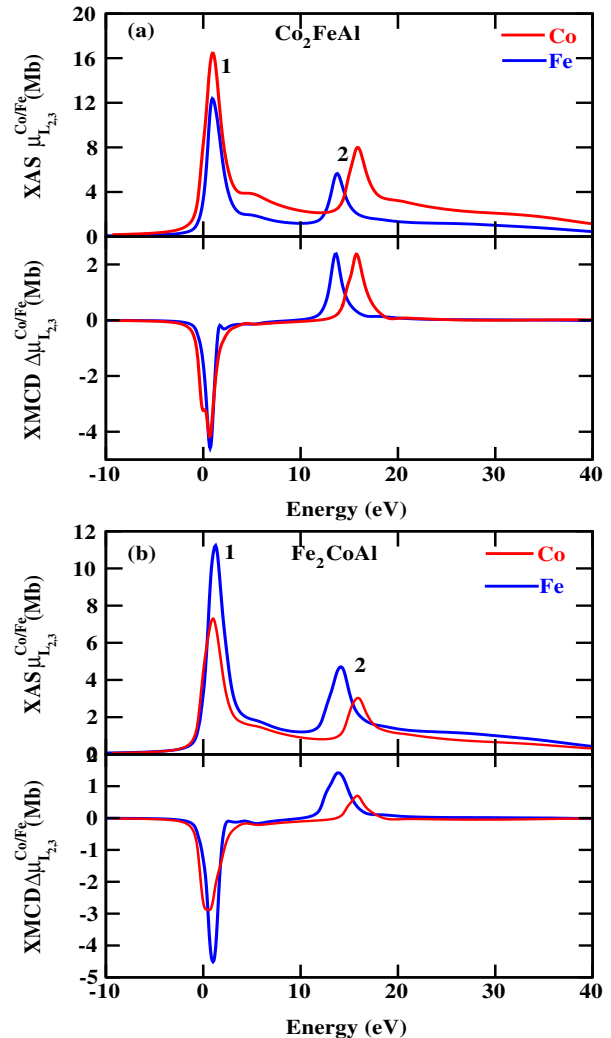


FIG. 5. XAS and XMCD of (a) Co_2FeAl and (b) Fe_2CoAl calculated within LDA+U

are shown in Fig.6 (a,b). Due to the presence of four atoms in a primitive cell, we can have twelve vibrational modes of phonon at any q -point, it consists of three acoustic modes and nine optical modes. The detail information about the dynamical stability of Co_2FeAl and Fe_2CoAl structure has been confirmed due to the absence of imaginary phonon frequencies [see Fig.6(a, b)]. For Co_2FeAl , the optical branches are located at 120.258 cm^{-1} , 215.194 cm^{-1} and 258.68 cm^{-1} at the Γ -point. For Fe_2CoAl , the optical branches are observed at 211.134 cm^{-1} , 228.466 cm^{-1} and 286.239 cm^{-1} along the Γ - point [Fig.6(b)]. However, we do not have sufficient data to compare our results for the same compounds, therefore we are compelled to compare with that of the analogous compounds Ru_2FeX ($X=\text{Si, Ge}$)⁷⁰. The reported value of optical branches⁷⁰ at Γ - point for Ru_2FeSi are 248.319 cm^{-1} , 253.221 cm^{-1} , 273.829 cm^{-1} , 289.636 cm^{-1} and 365.966 cm^{-1} and for Ru_2FeGe are 205.147 cm^{-1} , 215.651 cm^{-1} , 221.954 cm^{-1} , 232.458 cm^{-1} and 300.210 cm^{-1} . In

Compd.	M_{Co}	M_{Fe}	M_t^{Cal}	M_{Co}^*	M_{Fe}^*	M_t^{Rep}	M_{SP}	T_C^{cal}	T_C^{MFA}	T_C^{Expt}
CFA-GGA	1.236	2.757	4.99	1.2 ^a	2.8 ^a	5.08 ^a	5.0	926.2	1332.2	900 ^{d,e}
				0.79 ^g	2.77 ^g	4.82-5.22 ^b				1000 ^f
						4.25 ^g				1100 ^g
CFA-GGA+U	1.290	2.952	5.00				5	928		
FCA-GGA	1.118	2.559	5.05	1.0 ^a	2.5 ^a	5.14 ^a	4.0	937.05	1025.4	700-800 ^h
		1.64			1.6 ^a	4.91 ^c				
FCA-GGA+U	0.888	2.759	5.33				4.0	987.73		
		2.159								

TABLE II. Calculated partial magnetic moment of Co (M_{Co}), Fe (M_{Fe}) and Total Magnetic moment (M_t) in μ_B in comparison with the reported data (M^{Rep}) and Slater-Pauling rule (M_{SP}), Curie temperatures calculated from Eq.2 (T_C^{cal}) and Mean field approximation (T_C^{MFA}) in K, *denote other work (a ,b ,c ,d ,e ,f ,g ,h)

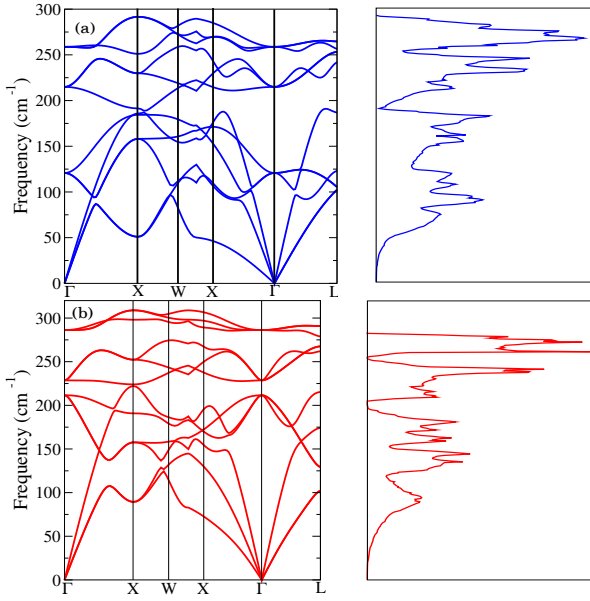


FIG. 6. Phonon dispersion & Phonon DOS of (a)Co₂FeAl (b) Fe₂CoAl

our calculation we have obtained only three optical branches at the Γ – point and degenerated into six modes along X-point. On the other hand, there are 5 distinct optical branches at Γ – point for Ru₂FeX which may be due to the presence of heavier Ru atom. As a result of heavier masses in Ru₂FeX, the optical and acoustic phonon couplings are strong and dominant⁷⁰. In our case the optical and acoustic phonon coupling is less derived due to the presence of low atomic masses.

VI. ELASTIC PROPERTIES

The validation of experimental elastic constant from the standard hypothesis gives further understanding about the possibility of synthesizes the closely resembling compounds. The computation of elastic constants and moduli of elasticity of a cubic Heusler compounds are simple and rudimentary

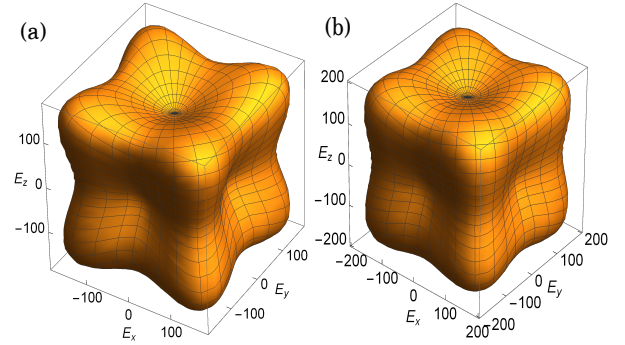


FIG. 7. The calculated 3D surface construction of Young's modulus in (a) Co₂FeAl and (b) Fe₂CoAl

which have been reported earlier in some of the articles⁷⁴⁻⁷⁷. The calculated elastic constants from cubic-elastic⁵⁰ code developed by Jamal et al. are presented in Table III. A necessary criteria for mechanical stability of the cubic crystal in relation to elastic constants are as follows;

$$C_{11} - C_{12} > 0, C_{44} > 0, (C_{11} + 2C_{12} > 0 \quad (5)$$

Our computed data of elastic constants strictly follows the above mentioned stability conditions(Eq.5). Therefore, both Co₂FeAl and Fe₂CoAl are Mechanically stable. The value of B/G=3.32 > 2.73 suggested that Co₂FeAl is more ductile as compared to Fe₂CoAl. Poisson's ratio (σ) is an important parameter to describe the nature of atomic bonding in the crystal. The $\sigma \sim 0.1$ refers to covalent bonding, moreover our calculated σ 's are 0.36 and 0.47 predict metallic bonding. The melting temperature of Fe₂CoAl is 1656.92 \pm 300 K higher than that of Co₂FeAl, 1390 \pm 300K. The hardness of a crystalline material is also a crucial factor in determining their practical applications and can be estimated from Young's modulus (Y). Young's modulus (Y) can also provide an information about the stiffness of a material, larger the Y values harder to deform. The results of direction dependences of Young modulus shows minima along the [100] axis (i.e., Y_X), [010] axis (i.e., Y_Y), [001] axis (i.e., Y_Z) and the maxima is located along [111] [see Fig.7(a,b)].

Compounds	C₁₁	C₁₂	C₄₄	B	G	B/G	Y	σ
*Co ₂ FeAl	243.09	141.64	138.59	209.27	62.86	3.32	171.426	0.36
*Fe ₂ CoAl	219.60	186.78	139.17	208.67	76.39	2.73	205.546	0.47
Fe ₂ CrAl ^a	229.56	151.41	275.94	177.46	181.267	0.979		
CASTEP (GGA) ^b	289.75	156.75	153.07	201.08	106.617	1.886		
CASTEP (LDA) ^b	258.24	134.78	139.14	177.09	99.21	1.785		
Co ₂ CrAl ^a	355.82	314.69	417.86	328.40	258.99	1.268		
Fe ₂ ScAl ^a	280.14	51.03	120.03	127.40	117.854	1.081		
Co ₂ ScAl ^a	180.16	162.26	150.86	168.23	94.141	1.787		
Co ₂ FeAl ^c	250.25	171.38	148.10	197.67	87.50	2.259	113.17	

TABLE III. Elastic constant (C_{ij}), Bulk Modulus, Shear Modulus (G), Youngs' modulus (Y) are in (GPa), B/G and Poisson's ratio (σ) in comparison with the available reported data. Here, * denote our results, ^a, ^b, ^c

VII. CONCLUSION

The electronic, magnetic, elastic and X-ray spectroscopic properties of Co_2FeAl and Fe_2CoAl have been computed from GGA and GGA+U functionals. Both L_{21} and $C1_b$ structures are stabilized by calculating the minimum energy corresponds to optimized lattice constants. The phonon dispersion relation as a function of frequency have been calculated to confirm their thermodynamical stability. The absence of imaginary phonon in the whole Brillouin zone of both L_{21} and $C1_b$ structures is a concrete proof of dynamical stability. Both Co_2FeAl and Fe_2CoAl possess strongly correlated d-electrons which can be treated more efficiently by the implementation of onsite Hubbard Coulomb potential (U) as GGA+U functional. On careful investigation of electronic properties we have found the blende of conducting and semi-conducting states, a finger print of typical half-metallicity in Co_2FeAl . Whereas Fe_2CoAl exhibit pure metallic behaviour with disperse Co-d and Fe d-states around the E_F . An integer value of total magnetic moment ($5.0 \mu_B$) is an additional testament of the half-metallicity in Co_2FeAl in accordance with the Slater-Pauling rule. However, for Fe_2CoAl the total magnetic moment deviate from the integer value defying

the Slater-Pauling rule. We have found an enhanced band gap in Co_2FeAl with the application of GGA+U. Wide band gap half-metals with high value of T_C (~ 1000 K) are critical factor for spintronic technology. The calculated values of T_C 's from Eq.2 are in close agreement with the experimental data where as the results from mean field approximation (MFA) are overestimated. The XAS and XMCD spectra are also calculated from LDA+U. Our result of XAS and XMCD spectra of Co_2FeAl are consistent with the available data. The $L_3:L_2$ ratio deviates from 2:1 branching ratio in Fe_2CoAl may be due to inaccurate choice of Coulomb potential (U). The elastic properties are highly crucial for the industrial application. The high value of $B/G > 2.0$, high σ and high melting temperature are credentials for practical application in device fabrication at high temperature.

VIII. ACKNOWLEDGEMENT

This project is jointly supported by DST & RFBR (under Indo-Russian joint project). Dr. D. P. Rai acknowledges Department of Science and Technology (DST) New Delhi, Govt. of India vide Lett. No. INT/RUS/RFBR/P-264. Prof. Genady M. Mikhailov acknowledges Russian Foundation for Basic Research, RFBR 17-57-45024.

* dibyaprakashrai@gmail.com

- ¹ A. Fert, The present and the future of spintronics, *Thin Solid Films* 517, 2 (2008).
- ² S. A. Wolf et al., Spintronics: A spin-based electronics vision for the future, *Science* 294, 1488 (2001).
- ³ S.D. Bader and S. Parkin, Spintronics, *Annu. Rev. Condens. Matter Phys.* 1 3.1, (2010).
- ⁴ J. F. Gregg, I. Petej, E. Jouguelet and C. Dennis, Spin electronics a review, *J. Phys. D: Appl. Phys.* 35, R121 (2002).
- ⁵ I. Zutic, J. Fabian, C. D. Sarma, Spintronics: fundamentals and applications, *Rev. Mod. Phys.* 76, 323 (2004).
- ⁶ S. Wurmehl, G. H. Fecher, H. C. Kandpal, V. Ksenofontov, and C. Felser *Appl. Phys. Lett.* 88, 032503 (2006)
- ⁷ Y. Wang, S. L. Shang, H. Fang, Z. K. Liu and L. Q. Chen, *Nat. Commun.* 2, 16006 (2016).
- ⁸ J. M. D. Coey, M. Venkatesan and C. B. Fitzgerald *Nature Mat.* 4(2005)173.
- ⁹ W. Z. Xiao, L. L. Wang, B. Meng and G. Xiao, *RSC-Advances*, 4, 39860 (2014).
- ¹⁰ T. Dietl, D. D. Awschalom, M. Kaminska, H. Ohno, *Spintronics in Semiconductors and Semimetals (Academic, 2008)*, vol. 82.
- ¹¹ S. Ishida, C. de Graff and R. Broer, *Phys. Rev. B* 75, 165116 (2007).
- ¹² R. A. de Groot, F. M. Mueller, P. G. van Engen and K. H. J. Buschow, *Phys. Rev. Lett.* 50, 2024 (1983).
- ¹³ A. Sadoc, C. de Graaf and R. Broer, *Phys. Rev. B*, 75, 165116 (2007)
- ¹⁴ F. G. Aliev, *Physica B*, 171, 199 (1991)
- ¹⁵ B. Deka and A. Srinivasan, *Phys. B:Condensed Matter* 121, 476 (2015).
- ¹⁶ D. P. Rai, J. Hashemifar, M. Jamal, Lalmuanpuia, M. P. Ghimire, Sandeep, D. T. Khathing, P. K. Patra, B. I. Sharma, Rosangliana

- and R. K. Thapa, *Ind. J. Phys.* 84,717-721 (2010).
- ¹⁷ A. H. Reshak, *RSC Adv.* 6, 54001-54012 (2016)
- ¹⁸ S. Sanvito, C. Oses, J. Xue, A. Tiwari, M. Zic, T. Archer, P. Tozman, M. Venkatesan, M. Coey and S. Curtarolo, *Sc. Adv.* 4, e1602241 (2017).
- ¹⁹ S. Trudel, O. Gaier, J. Hamrle and B. Hillebrands, *J. Phys. D: Appl. Phys.* 43, 193001 (2010).
- ²⁰ A. Boocheani, B. Nowrozi, J. Khodadadi, S. Solaymani, and S. J. Asadabadi, *J. Phys. Chem. C*, 121 (7) 3978-3986 (2017).
- ²¹ J. Kbler, G. H. Fecher and C. Felser, *Physical Review B* 76, 024414 (2007)
- ²² K. H. J. Buschow and P. G. van Engen, *J. Magn. Magn. Mater.* 25,90 (1981)
- ²³ P. G. van Engen, K. H. J. Buschow, and M. Erman, *J. Magn. Magn. Mater.* 30, 374 (1983)
- ²⁴ P. J. Webster, *J. Phys. Chem. Solids* 32, 1221 (1971)
- ²⁵ K. R. A. Ziebeck and K.-U. Neumann, in *Alloys and Compounds of d-Elements with Main Group Elements*, edited by H. P. J. Wijn, Landolt-Brnstein, New Series Group III, Vol. 32, Pt. C Springer-Verlag, Heidelberg, 2001, Pt. 2, pp. 64314.
- ²⁶ R. Y. Umetsu, K. Kobayashi, A. Fujita, K. Oikawa, R. Kainuma, K. Ishida, N. Endo, K. Fukamichi, and A. Sakuma, *Phys. Rev. B* 72, 214412 (2005)
- ²⁷ I. Galanakis and Ph. Mavropoulos, *J. Phys.: Condens. Matter*, 19 315213 (2007).
- ²⁸ R. J. Soulen Jr., J. M. Byers, M. S. Sossfsky, B. Nadgorny, T. Ambrose, S. F. Cheng, P. R. Broussard, C. T. Tanaka, J. Nowak, J. S. Moodera, A. Barry and J. M. D. Coey, *Science* 282, 85 (1998).
- ²⁹ H. Kato, T. Okuda, Y. Okimoto, Y. Tomioka, K. Oikawa, T. Kamiyama, Y. Tokura, *Phys. Rev. B* 69, 184412 (2004).
- ³⁰ D.P. Rai, A. Shankar, M.P. Ghimire, Sandeep, R.K. Thapa, *Comp. Mat. Sc.* 101, 313-320 (2015).

- ³¹ T. Shishidou, A. J. Freeman, R. Asahi, *Phys. Rev. B* 64, 180401 (2001).
- ³² C. Y. Fong, M. C. Qian, J. E. Pask, L. H. Yang, S. Dag, *Appl. Phys. Lett.* 84, 239 (2004).
- ³³ A. Hirohata, J. Sagar, L. R. Fleet, S. S. P. Parkin. Heusler Alloy Films for Spintronic Devices. In: C. Felser, A. Hirohata (eds) *Heusler Alloys*. Springer Series in Materials Science, vol 222. Springer, Cham (2016).
- ³⁴ J. Enkovaara, A. Ayuela, A. Zayak, P. Entel, L. Nordstrom, M. Dube, J. Jalkanen, J. Impola and R. Nieminen, *Mater. Sc. Eng.* 60, 378 (2004).
- ³⁵ G. van der Laan and E. Arenholz, *The European Physical Journal Special Topics*, 169 (1), 187-190 (2009).
- ³⁶ T. Jo and G. A. Sawatzky, *Phys. Rev. B* 43, 87718774 (1991).
- ³⁷ C. Piamonteze, P. Miedema, and F. M. F. de Groot, *Phys. Rev. B* 80, 184410 (2009)
- ³⁸ D. P. Rai and C. E. Ekuma and A. Boochani and S. Solaymani and R. K. Thapa, *J. Appl. Phys.* 123, 161509 (2018).
- ³⁹ Y. I. Matsushita, G. Madjarova, J. K. Dewhurst, S. Shallcross, C. Felser, S. Sharma and E. K. U. Gross, *J. Phys. D: Appl. Phys.* 50, 095002 (2017)
- ⁴⁰ P. Giannozzi, S. Baroni, N. Bonini, M. Calandra, R. Car, C. Cavazzoni, D. Ceresoli, G.L. Chiarotti, M. Cococcioni, I. Dabo, et al., *J. Phys. Condens. Matter* 21, 395502 (2009)
- ⁴¹ F. D. Murnaghan, *Proc. Natl. Acad. Sci. USA*, 30, 244 (1944)
- ⁴² S. Baroni, S. De Gironcoli, A. Dal Corso, P. Giannozzi, *Rev. Mod. Phys.* 73, 515 (2001)
- ⁴³ X. Gonze, C. Lee, *Phys. Rev. B* 55, 10355 (1997)
- ⁴⁴ G. Kresse and D. Joubert, *Phys. Rev. B* 59, 1758 (1999)
- ⁴⁵ J. P. Perdew, K. Burke, and M. Ernzerhof, *Phys. Rev. Lett.* 77, 3865 (1996)
- ⁴⁶ H. J. Monkhorst, J. D. Pack, *Phys. Rev. B* 13, 5188 (1976).
- ⁴⁷ D.P. Rai, A. Shankar, Sandeep, L.R. Singh, M. Jamal, S.J. Hashemifar, M.P. Ghimire, R.K. Thapa, *Armenian Journal of Physics* 5, 105 (2012)
- ⁴⁸ H. Ebert, D. Kodderitzsch, and J. Minar, *Reports on Progress in Physics* 74 (9), 096501 (2011).
- ⁴⁹ H. Ebert, *Fully Relativistic Band Structure Calculations for Magnetic Solids - Formalism and Application*, 191-246 (Springer Berlin Heidelberg, Berlin, Heidelberg, 2000), ISBN 978-3-540-46437.
- ⁵⁰ M. Jamal, S. J. Asadabadi, I. Ahmad and H.A. Rahnamaye Aliabad, *Comput. Mat. Sc.* 95, 592-599 (2014).
- ⁵¹ S. Husain, A. Akansel, S. Kumar, P. Svedlindh and S. Chaudhary, *Sc. Rep.* 432, 28692 (2016).
- ⁵² M. Csanad, T. Csorgo, and B. Lorstad, *Neukleonika*, 49, S49 (2004).
- ⁵³ D. Comtesse, B. Geisler, P. Entel, P. Kratzer and L. Szunyogh, *Phys. Rev. B.* 89, 094410 (2014).
- ⁵⁴ M. Gilleben and R. Dronkowski, *J. Comput. Chem.* 30, 1290-1299 (2009).
- ⁵⁵ Silvia Picozzi and Arthur J Freeman, *J. Phys.: Condens. Matter* 19, 315215 (2007)
- ⁵⁶ I. Galanakis, E. Sasoglu, S. Blugel, and K. Ozdogan, *Phys. Rev. B*, 90, 064408 (2014)
- ⁵⁷ S. Wurmehl, G. H. Fecher, V. Ksenofontov, F. Casper, U. Stumm, C. Felser, H.-J. Lin, and Y. Hwu, *J. Appl. Phys.* 99, 08J103 (2005)
- ⁵⁸ X. -Q Chen, R. Podloucky, and P. Rogl, *J. Appl. Phys.* 100, 113901 (2006)
- ⁵⁹ A. I. Liechtenstein, M. I. Katsnelson, V. P. Antropov, and V. A. Gubanov, *J. Magn. Magn. Mater.* 67, 65 (1987).
- ⁶⁰ K. Sato, W. Schweika, P. H. Dederichs, and H. Katayama-Yoshida, *Phys. Rev. B* 70, 201202 (2004).
- ⁶¹ L. Bergqvist, O. Eriksson, J. Kudrnovsky, V. Drchal, P. Korzhavyi, and I. Turek: *Phys. Rev. Lett.* 93, 137202 (2004).
- ⁶² D. Ebke, Z. Kugler, P. Thomas, O. Schebaum, M. Schafers, D. Nissen, J. Schmalhorst, A. Hutten, E. Arenholz, A. Thomas, *IEEE Trans. Magnetics*, 46, 1925-1928 (2010).
- ⁶³ H. Wende, A. Scherz, C. Sorg, K. Baberscheke, E. K. U. Gross, H. Appel, K. Burke, J. Minr, H. Ebert, A. L. Andukinov and J. J. Rehr, Chapter in *X-ray Absorption Fine Structure*, Conference XAFS13 78, (2007).
- ⁶⁴ J. Schwitalla and H. Ebert, *Phys. Rev. Lett.* 80, 4586 (1998).
- ⁶⁵ S. Soni, S. Dalela, S.S. Sharma, E.K. Liu, W.H. Wang, G.H. Wu, M. Kumar, K.B. Garg, *J. Alloys Compd.*, 674 295-299 (2016).
- ⁶⁶ J. Hasier et al., *EPJ Techniques and Instrumentation*, 4, 5 (2017).
- ⁶⁷ A. Kumar et al. *Phys. B* 96, 224425 (2017).
- ⁶⁸ M. Belmehuenai, et al. *J. Appl. Phys.* 115, 043918 (2014).
- ⁶⁹ W. H. Wang et al., *Phys. Rev. B* 82, 092402 (2010).
- ⁷⁰ M. Rizwan, A. Afaq, A. Aneza, *Physica B* 537, 225-227 (2018)
- ⁷¹ N. Arkan, A. yigr, A. Candan, . Uur, Z. Charifi, H. Baaziz and G. Uur, *J. Mat. Sc.* (2014).
- ⁷² X. L. Niu, L. J. Wang, *Comput. Mater. Sci.* 53, 128-132 (2012).
- ⁷³ B. Fadila, M. Ameri, D. Bensaid, M. Noureddine, I. Ameri, S. Mesbah, Y. Al-Douri, *J. Magn. Magn. Mater.* 448, 208-220 (2018).
- ⁷⁴ A. Reuss, *Z. Angew. Math. Mech.* 9, 49-58 (1929).
- ⁷⁵ W. Voigt, *Lehrbuch der kristallphysik (mit ausschuss der kristaloptik)*, Springer-Verlag, (2014).
- ⁷⁶ R. Hill, The elastic behaviour of a crystalline aggregate, *Proc. Phys. Soc. Sect. A.* 65, 349 (1952).
- ⁷⁷ F. Mouhat, F.-X. Coudert, *Phys. Rev. B.* 90, 224104 (2014).